

Lactoferrin improves cognitive function and attenuates brain senescence in aged mice

Jiaping Zheng^{b,1}, Yunzhen Xie^{a,1}, Fei Li^c, Yu Zhou^a, Liqin Qi^b, Libin Liu^{b,*}, Zhou Chen^{a,*}

^a School of Pharmacy, Fujian Medical University, Fuzhou 350122, China

^b Department of Endocrinology, Fujian Medical University Union Hospital, Fuzhou 350001, China

^c Department of Pharmacy, Fujian Provincial Hospital, Fuzhou 350001, China

ARTICLE INFO

Keywords:

Lactoferrin
Aged mice
Cognitive function
Reactive oxygen species
Metabolites

ABSTRACT

Lactoferrin (LF) has been shown to be effective in attenuating some aging-related changes, although its potential in alleviating aging-related cognitive decline remains to be clarified. In this study, we evaluated the effects of LF (2000 mg/kg/day for 3 months) on the cognitive ability of 16-month-old C57/BL6J mice. Spatial cognition was improved in aged mice after LF administration, with more pyramidal cells detected in the hippocampi, and more regular distribution. LF also reduced iron deposition, malondialdehyde (MDA) and ROS levels in the hippocampus. Similarly, LF decreased the expression of two subunits of NADPH oxidase: *Gp91phox* and *P22phox*, and reduced hippocampal and serum levels of IL-1 β , IL-6 and TNF- α in aged mice. Metabolomic analysis revealed alterations in LysoPG, LysoPS, xanthine, adenosine and oxypurinol, which were partially reversed by LF. The potential of LF to protect cognitive function in aged animals offers a unique pharmacological approach for neurodegenerative disorders associated with aging.

1. Introduction

It has been estimated that by 2050, the number of people aged over 60 years will reach almost 2.1 billion (Wyss-Coray, 2016), representing a significant burden both on individuals and society. Aging is a universal change throughout the body, and the process of aging is accompanied by a decline in brain function and cognitive abilities (Mattson & Magnus, 2006).

Reactive oxygen species (ROS) are a class of partially reduced oxygen containing molecules, including superoxide, peroxides (H₂O₂ and ROOH) and free radicals. The accumulation of ROS accompanies the aging process and results in mitochondrial dysfunction and genomic damage (Saraswat & Rizvi, 2017; Wang & Hekimi, 2015); ROS accumulation also increases lipid peroxidation and glycoxidation, giving rise to elevated endogenous production of reactive aldehydes and their derivatives, such as glyoxal, methylglyoxal (MG), malonic dialdehyde (MDA), and 4-hydroxy-2-nonenal (HNE). These molecules are further converted into advanced lipoxidation and glycation end products (ALEs and AGEs, respectively), leading to protein cross-linking, cellular

malfunctions and even cell death (Moldogazieva, Mokhosoev, Mel'nikova, Porozov, & Terentiev, 2019). Aging is also characterized by an elevated level of universal inflammation and increased inflammatory cytokine release, which is initiated and exacerbated by oxidative stress (Guzik & Touyz, 2017). The CNS is also affected by peripheral inflammation, which contributes to neuronal damage in the hippocampus and cortex, and is closely related to cognitive deficits and memory loss (Au et al., 2016; Di Benedetto, Muller, Wenger, Duzel, & Pawelec, 2017).

Another feature that accompanies aging is disturbed iron homeostasis, which is manifested as unusual and excessive iron deposition in aged brains and is also related to impaired cognition and neurodegenerative diseases (Daugherty & Raz, 2015; Dixon & Stockwell, 2014; Sala-Llonch et al., 2017; Zucca et al., 2017). Iron overload has been reported to be closely related to cellular senescence (Yan, Michel, Anne, & Bernard, 2019). The labile iron (or redox-active iron) existing in the mitochondrial matrix and cytosol is capable of directly catalyzing free radical formation via Fenton chemistry (Kell, 2009; Muñoz, Carrasco, Campos, Aguirre, & Núñez, 2016). The incorporation of iron and its

Abbreviations: HE, hematoxylin and eosin; LC-MS, liquid chromatography-mass spectrometry; LF, lactoferrin; LysoPG, lysophosphatidylglycerol; LysoPS, lysophosphatidylserine; MDA, malondialdehyde; MWM, Morris Water Maze; PCA, principal component analysis; PLS-DA, partial least squares-discriminant analysis; ROS, reactive oxygen species; SOD, superoxide dismutase

* Corresponding authors.

E-mail addresses: libinliu@fjmu.edu.cn (L. Liu), chenzhou@fjmu.edu.cn (Z. Chen).

¹ Co-first authors.

<https://doi.org/10.1016/j.jff.2019.103736>

Received 4 September 2019; Received in revised form 30 November 2019; Accepted 6 December 2019

Available online 29 December 2019

1756-4646/ © 2019 The Authors. Published by Elsevier Ltd. This is an open access article under the CC BY-NC-ND license (<http://creativecommons.org/licenses/by-nc-nd/4.0/>).

derivatives is vital for the activity of ROS-producing enzymes, such as NADPH oxidases (NOXs) and xanthine oxidase (Toshitaka, Isao, & Hidenori, 2019; Yauger et al., 2019).

Lactoferrin (LF) is an 80 kD naturally occurring milk-derived glycoprotein that exists ubiquitously in body fluids, including milk, tears, saliva, vaginal fluids and semen (van der Strate, Beljaars, Molema, Harmsen, & Meijer, 2001). LF is also released by polymorphonuclear neutrophils in response to inflammatory stimuli and takes part in the defense against infectious agents (Drago-Serrano, Campos-Rodríguez, Carrero, & De, 2017). LF consists of a simple polypeptide chain folded into two lobes, each of which reversibly binds Fe^{2+} or Fe^{3+} to form apo-LF, or the iron moieties are released to form holo-LF (Gonzalez-Chavez, Arevalo-Gallegos, & Rascon-Cruz, 2009). The anti-bacterial activity of LF was among the first functions to be elucidated and is based on its ability to sequester iron and interact with infectious agents to exert immunomodulatory functions (Dominique, Elizabeth, Mathireu, & Joel, 2006; Drago-Serrano et al., 2017). Furthermore, LF readily crosses to the blood-brain-barrier, and has been shown to ameliorate mitochondrial dysfunction and reduce cellular damage by scavenging ROS in animal models of Alzheimer's disease (Guo et al., 2017; Park et al., 2013). In light of the multifunctional capacities of LF in alleviating aging-related cellular damage, it is reasonable to hypothesize that LF might also exert protective effects on the aging brain; however, the studies in this field are scarce.

In this study, 16-month-old mice were randomly assigned to the aged group and the aged + LF group (treated with LF for 3 months); 2-month-old mice served as young controls. We evaluated the effects of orally administered LF on the cognitive ability of naturally aged mice, and compared the redox and inflammatory statuses in the three groups of mice. We conducted a liquid chromatography-mass spectrometry (LC-MS)-based analysis of the metabolomic profiles of these three groups of mice and provided insights into the possible mechanisms of the effects of LF on the brains of aged mice.

2. Materials and methods

2.1. Animals and drug administration

Female C57/BL6J mice were purchased from Beijing Vital River Laboratory Animal Technology (China) and housed (5 mice per cage) in a well-ventilated and pathogen-free environment with a 12-h light:dark cycle and free access to food and water. All mice were maintained under standard laboratory conditions with humidity at 40–60% and temperature at 20 ± 3 °C. At 16-months-old, the mice were randomly assigned to an aged group and an aged + LF group; 2-month-old mice were used as young controls ($n = 16$ mice per group). All operations were conducted in accordance with the ARRIVE guidelines, the National Institutes of Health Guide for the Care and Use of Laboratory Animals (NIH eighth edition, revised 2011) and Institutional Animal Care and Use Committee of Fujian Medical University (No. FJMU IACUC 2018-034).

LF powder (HBW180903-2, Hubei Widely Chemical Technology, China) was dissolved in 0.9% saline to a final concentration of 0.2 g/mL. Hou reported that the optimal intragastric intervention dose of LF in Sprague–Dawley rats was 1000 mg/kg/day (Hou, Xue, & Lin, 2012). Based on the Rat Mouse Equivalent Dose Conversion Principle, the equivalent dose of LF used in mice was 2000 mg/kg/day. The mice in the aged + LF group received 2000 mg/kg/day LF by gavage for 3 months (Guo et al., 2009), while the mice in the aged and young groups received an equal amount of 0.9% saline according to the same regimen. At the end of the intervention, the mice were euthanized with 100 mg/kg pentobarbital sodium administered intraperitoneally (Xinwei et al., 2019). For HE staining and Perl's staining, the mice were anesthetized with 60 mg/kg of pentobarbital sodium administered intraperitoneally (Erika B & Steven S, 2013), and then perfused via the cardiac apex with 0.9% saline followed by 4% paraformaldehyde in

0.1 M phosphate buffer solution (PBS), and brain tissues were dissected and fixed in 4% paraformaldehyde. For quantitative real-time PCR (RT-qPCR), metabolomic analysis, enzyme-linked immunosorbent assays (ELISA), and tests for malondialdehyde (MDA) and superoxide dismutase (SOD) activity, the mice were decapitalized, and the brains were removed and hippocampi were dissected on the ice. The blood samples were stored at 4 °C overnight and then, both blood and hippocampus samples were stored at -80 °C.

2.2. Morris water maze (MWM) tests

The MWM tests were performed according to a previously reported protocol (Vorhees & Williams, 2006). A circular pool (120 cm diameter) was used for the MWM test, with a transparent platform submerged 1 cm under water in a fixed position. Water was made opaque with non-toxic white paint. During the test, the pool was surrounded by a curtain to eliminate any influence from observers and spatial cues were arranged in fixed positions around the pool. In the acquisition phase, the mouse was released into the pool and allowed to swim for 60 s. Mice that found the platform voluntarily were allowed to remain there for 10 s and then returned to their cages, while mice that failed to find the platform in the required time were gently guided onto the platform and retained on it for 10 s. Each mouse underwent four trials each day for consecutive 5 days, and was released from different quadrants in each trial. On day 6, the platform was removed, and the mouse was released from the quadrant opposite to the original position of the platform and allowed to search in the water for 60 s. The swimming tracks, escape latencies, and swimming speeds of mice and times of crossing the target spot on each of the six days were recorded and analyzed using SAMRT 2.0 (Pan Lab, Barcelona, Spain). Each time the mice finished swimming, they were dried with a towel and kept warm with a heating installation. For MWM tests, 10 mice were included in each group.

2.3. HE staining

For the HE staining, the tissues were embedded in paraffin, then sectioned using a microtome (RM2016, Leica, Germany) to obtain 4- μm -thick hippocampus sections, which were washed with distilled water and stained with alum hematoxylin for 3 min. Next, the sections were rinsed in ascending concentrations of acid alcohols (85–95%), stained with eosin for 5 min, and then dehydrated for further observation.

2.4. Perl's staining

For Perl's staining of ferric iron (Fe^{3+}), the brain sections were dehydrated in ascending concentrations of acid alcohol (85–95%) and then incubated in a solution containing equal amount of 2% potassium ferrocyanide and hydrochloric acid (HCl) for 30 min. After washing three times with distilled water, sections were incubated with 3,3'-diaminobenzidine (DAB) for 30 min to visualize the stain. The sections were then rinsed with alum hematoxylin for 1 min, washed with distilled water, dehydrated in an ethanol series, cleared with xylene and then cover-slipped.

The sections of HE staining and Perl's staining were observed using a microscope (Eclipse E100, Nikon Instruments Inc., Tokyo, Japan), and Panoramic DESK (P-MIDI, P250, P1000, 3D HISTECH) was used to scan the histological sections, and the Panoramic Scanner was used to generate microphotographs.

2.5. Assays for MDA levels and SOD activity

The hippocampus tissues were thawed on ice before the addition of ice-cold PBS (9 mL PBS to 1 mg of tissue). After being homogenized, the tissues were centrifuged at 5000g for 10 min at 4 °C. The supernatant was removed for the protein concentration determination using the

bicinchoninic acid assay (BCA assay, P0012S, Beyotime Biotechnology, Jiangsu, China). The MDA level and SOD activity in hippocampus tissue were determined using MDA (A003-1, TBA method) and SOD (A001-3, WST-1 method) assays kits, respectively (Nanjing Jiancheng Bioengineering Institute, China) according to the manufacturer's instructions. Data were presented as the ratio of the MDA level or SOD activity in the aged and aged + LF group to that in the young group.

2.6. Elisa

Hippocampal tissues were rinsed with ice-cold PBS to remove excess blood, and then homogenized in PBS (9 mL PBS to 1 mg of tissue) with a glass homogenizer on ice. After centrifugation for 5 min at 5000g, the supernatants were processed using mouse ROS ELISA kit (ml009876-C, Shanghai Enzyme-linked Biotechnology Co., Ltd, China) according to the manufacturer's instructions.

Blood samples were collected using serum separator tubes (BD™ P100 Blood Collection System) and stored overnight at 4 °C. The samples were then centrifuged for 20 min at 1000g for isolation of the serum. Hippocampal and serum levels of IL-1β, IL-6 and TNF-α were assayed using mouse IL-1β ELISA kit (ml063132-C, Shanghai Enzyme-linked Biotechnology Co., Ltd), mouse IL-6 ELISA kit (ml002293-C, Shanghai Enzyme-linked Biotechnology Co., Ltd), and mouse TNF-α ELISA kit (ml002095-C, Shanghai Enzyme-linked Biotechnology Co., Ltd) according to the manufacturer's instructions.

2.7. RT-qPCR

RNA was extracted from hippocampal tissues using the Easy Spin Plus kit (RN28, Aidlab Biotechnologies, China) according to the manufacturer's instructions. RNA (1 mg) was reverse-transcribed using an Arktik Thermal Cycler (AKC481201135, Thermo Fisher) with the PrimeScript™ RT reagent kit (RR037A, TaKaRa, Beijing, China) and primers (DNA sequence 5'–3') synthesized by Sangon Biotech, China (Table 1). cDNA was amplified in a reaction volume of 20 μL on a LightCycler 96 real-time PCR instrument (Roche). The reaction volume was composed of 10.0 μL of TB Green PremixExTaqII (RR820A, TaKaRa), 0.8 μL of each amplification primer (10 pmol/mL), 6.4 μL of nucleic acid-free water and 2 μL of cDNA. The thermal cycling was carried out as follows: denaturing and polymerase hot-start activating step at 95 °C for 30 s, followed by 40 repeated cycles of 95 °C for 5 s and 60 °C for 20 s. Melting curves were constructed by increasing the final temperature from 60 °C to 95 °C. Samples were assayed in triplicate, and each assay was repeated three times. Data were analyzed using the comparative cycle threshold (Ct) method (ΔΔCt), and β -actin was used as an internal control. These steps were conducted in accordance with the latest Publication of Quantitative Real-Time PCR Experiments (MIQE) guidelines (Plain et al., 2014).

2.8. Hippocampal metabolomic analysis via LC-MS

The hippocampal samples were thawed on ice, and every 20 μL of sample was extracted with 120 μL of precooled 50% methanol buffer.

Table 1
Primer sequences for RT-qPCR.

Gene		Primer sequence
<i>P22phox</i>	Forward	5'-CCATTGCCAGTGTGATCTATCT-3'
	Reverse	5'-TTGGTAGGTGGTTGCTTGAT-3'
<i>Gp91phox</i>	Forward	5'-GACAGGAACCTCACTTCCATA-3'
	Reverse	5'-TGAAGAGATGTGCAATTGTGTG-3'
<i>Xdh</i>	Forward	5'-TTCAAACCTTTAGATCCCACCC-3'
	Reverse	5'-GGGCAGATGATCAGAGGAAATA-3'
β -actin	Forward	5'-GGAGATTACTGCCCTGGCTCCTA-3'
	Reverse	5'-GACTCATCGTACTCTGCTTGCTG-3'

The mixture was vortexed for 1 min, incubated at room temperature for 10 min, and then stored overnight at –20 °C. After centrifugation at 4000g for 20 min, the supernatants were transferred into new 96-well plates. Quality control (QC) samples were prepared by mixing 10 μL of each extraction mixture.

All samples were evaluated by the LC-MS using an ultra-performance liquid chromatography (UPLC) system (SCIEX, Framingham, MA, USA) operated according to the manufacturer's instructions and coupled with a high-resolution tandem mass spectrometer TripleTOF5600plus (SCIEX, Framingham, MA, USA) for chromatographic separation and metabolites detection. Samples (4 μL) were injected into an ACQUITY UPLC T3 column (100 mm × 2.1 mm, 1.8 μm, Waters, UK), and the temperature of the column was maintained at 35 °C. The mobile phase consisted of solvent A (water, 0.1% formic acid) and solvent B (Acetonitrile, 0.1% formic acid), with the flow rate set at 0.4 mL/min and the gradient elution conditions set as follows: 0–0.5 min, 5% B; 0.5–7 min, 5% to 100% B; 7–8 min, 100% B; 8–8.1 min, 100% to 5% B; 8.1–10 min, 5% B.

The mass spectrometry data were acquired in IDA mode. The survey scans were acquired in 150 ms and the total cycle time was fixed at 0.56 s. Four-time bins were summed for each scan at a pulse frequency of 11 kHz by monitoring the 40 GHz multichannel TDC detector with four-anode/channel detection. During the acquisition, the mass accuracy was calibrated every 20 samples and a QC sample was acquired in the interval between every 10 samples. The operation parameters were set as follows: curtain gas, 30 PSI; ion source gas, 60 PSI (ion source gas 1), 60 PSI (ion source gas 2); interface heater temperature, 650 °C; spray voltage, 5.0 kV (ESI+) or –4.5 kV (ESI–).

The data acquired were processed using XCMS version 3.4.1, CAMVER version 1.38.0, metaX version 1.4.16 toolbox and R software. Annotations of metabolites were achieved by matching the exact molecular mass data (m/z) of samples with the online Kyoto Encyclopedia of Genes and Genomes (KEGG; <https://www.kegg.jp>) and Human Metabolome Database (HMDB; <http://www.hmdb.ca/>). A metabolite was annotated if the difference between the observed and the database mass values was less than 10 ppm. The molecular formula of the metabolite was further validated according to the isotopic distribution measurements, and an in-house fragment spectrum library of metabolites was also used for the metabolite identification. The extraction of peak intensity data, peak alignment and normalization were achieved using XCMS, and those detected in less than 50% of QC samples or 80% of biological samples were removed. Signal intensity drift was minimized by fitting QC-based robust LOESS signal correction to the QC data with respect to the order of injection. In addition, the relative standard deviations of the metabolic features were calculated across all QC sample, and those with relative standard deviations > 30% were removed.

The dataset of the molecular features was imported into MetaboAnalyst 2.0 (<http://www.metaboanalyst.ca/>) for statistical analysis (Jasmine, Mai, & Jianguo, 2019). Principal component analysis (PCA) and partial least squares-discriminant analysis (PLS-DA) were performed after autoscaling. The metabolite features with variable importance in projection (VIP) > 1 in PLS-DA were used to select for discriminating variables among the three groups. The robustness of the model was evaluated by standard cross-validation using a random permutation test (200 iterations). The extracted R^2 and Q^2 values reflected the explained variance and predictive capabilities, respectively. The metabolites screened by multivariate statistical analysis were validated at a univariate level, using Student's t -test with the critical P -value was adjusted for multiple tests by the false-discovery rate (FDR, Benjamini–Hochberg) test. $P < 0.05$ was considered to indicate statistical significance.

2.9. Statistical analysis

All data were represented as means \pm standard error of the mean

(SEM). IBM SPSS Statistics 20.0 and GraphPad Prism 5.0 program for Windows (GraphPad Software, San Diego, CA, USA) were used for data analysis and diagrams. For the analysis of MWM data, the distribution was assessed using the Kolmogorov–Smirnov test, and the relationships among repeated measured data were examined using Mauchly’s test, and two-way repeated measures analysis of variance (ANOVA) of the general linear model was used to compare the training trials among different groups. For the behavioral probe data and other visibility trial data, one-way ANOVA was used for comparisons among three groups if the data were normally distributed, or Kruskal-Wallis rank sum tests were performed if the data were not normally distributed. $P < 0.05$ was considered to indicate statistical significance.

3. Results

3.1. Spatial cognition of aged mice was improved by LF administration

Escape latency and number of platform crosses were evaluated to assess the spatial learning and memory retrieval ability of mice. There were no significant differences in the average swimming speeds determined during 6 days of tests among the three groups. In the acquisition phases, escape latencies showed that the aged mice spent significantly more time in searching for the platform ($P < 0.001$; Fig. 1A). Compared with the young group, the escape latencies in the aged group began to increase on day 2 and the difference persisted to the end of the acquisition phases, indicating a decline in the spatial learning ability. This effect of aging was partially rescued by LF ($P < 0.01$; Fig. 1A). Similarly, the number of platform crosses revealed that the aged mice exhibited impaired spatial memory retrieval ability (decreased by 64.71%, $P = 0.001$; Fig. 1B), which was also partially restored by LF (increased by 100%, $P = 0.039$; Fig. 1B).

3.2. Histological features of the CA1 subregion of hippocampi in aged mice were improved by LF administration

We next evaluated the histological alterations in the three groups (Fig. 2). The microscopic structure of the hippocampal CA1 region in the young group was clear, with 3–4 layers of pyramidal cells arranged in a compact formation and a large, round nucleus, with 1–2 clearly visible nucleoli. In contrast, the pyramidal cells of the aged group were arranged loosely and fewer in number (reduced by 25.82%, $P = 0.003$; Fig. 2B). Compared with the aged group, the aged + LF group contained relatively abundant pyramidal cells in the CA1 region (increased by 48.90%, $P < 0.001$; Fig. 2B). The results showed that the pyramidal cells in the mouse hippocampus were partially lost with age, suggesting the existence of adverse events that resulted in the damage to neurons, and the capacity of LF to compensate partially for such damage.

3.3. Brain iron deposits of aged mice were decreased by LF administration.

Excessive deposition of ferric iron (Fe^{3+}) in the brain has been implicated in impaired brain functions in both aging and age-related neurodegenerative diseases (Muñoz et al., 2016; Zucca et al., 2017). In this study, young mice showed little visible brain Fe^{3+} deposits, whereas aged mice exhibited diffuse Fe^{3+} deposition in the extracellular space of hippocampus region (increased by 212.31%, $P = 0.006$; Fig. 3C), as well as increased Fe^{3+} -positive neuronal cells in the hippocampi (increased by 42.86%, $P < 0.001$; Fig. 3B). However, the Fe^{3+} -positive region in the brain of aged mice treated with LF was notably reduced (decreased by 52.71%, $P = 0.002$; Fig. 3C).

3.4. Oxidative stress in the brains of aged mice was alleviated by LF administration

As markers of oxidative stress, we tested MDA and ROS contents and SOD activity in hippocampus tissues of mice in the three groups. As

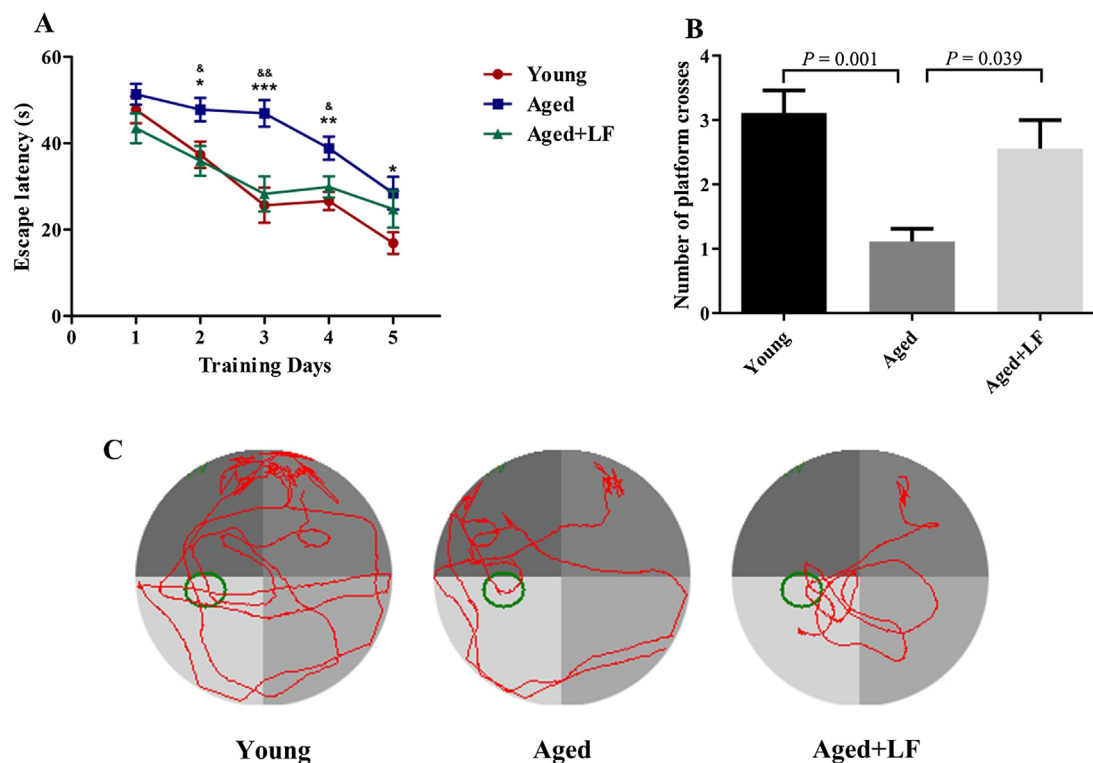


Fig. 1. Lactoferrin improves spatial cognition in aged mice. (A) Escape latency. (B) Crossings of the target quadrant during the probe trial. (C) Representative swimming tracks of different groups of mice in the probe trial. $n = 10$ mice per group. * $P < 0.05$, ** $P < 0.01$, *** $P < 0.001$ vs. young group; & $P < 0.05$, && $P < 0.01$ vs. aged + LF group.

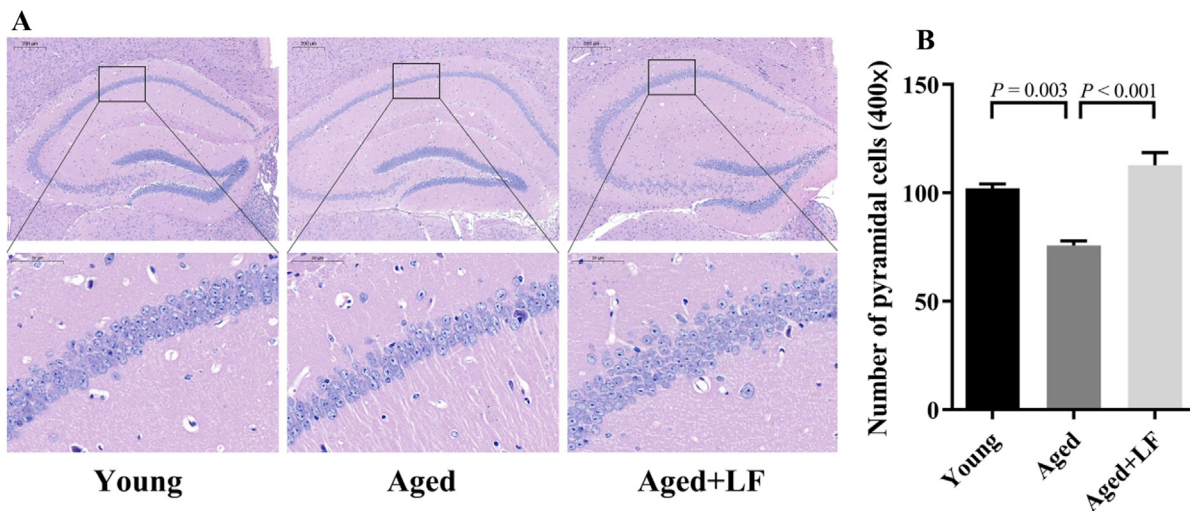


Fig. 2. Lactoferrin improves the histological features in the hippocampal CA1 subregion in aged mice. Hematoxylin and eosin staining showing the histological alterations in the hippocampal CA1 region. Scale bar = 200 μm . Enlarged images are shown in the lower column. Scale bar = 50 μm . (B) The numbers of pyramidal cells in the hippocampal CA1 subregion were counted in three different fields under 400 \times magnification. $n = 3$ mice per group.

shown in Fig. 4, aged mice exhibited higher levels of ROS and MDA (increased by 41.08% and 30.00%, $P < 0.001$ and $P = 0.038$, respectively), but lower levels of SOD activity (decreased by 8.13%, $P = 0.001$), indicating exacerbated oxidative stress in the brain of aged mice, and impaired anti-oxidative strength. After LF intervention, ROS and MDA levels were reduced (decreased by 16.38% and 20.99%, $P < 0.01$ and $P = 0.039$, respectively), while SOD activity was up-regulated (increased by 3.85%, $P = 0.019$), indicating the ability of LF to alleviate oxidative stress and restore anti-oxidative capacity.

To evaluate the impact of LF on NADPH oxidase, which catalyzes

ROS production, we analyzed the expression of the prototype of NADPH oxidase, *Gp91phox* (also known as *Nox2*), and its catalytically active subunit, *P22phox* (Bedard & Krause, 2007). As shown in Fig. 4D and E, aged mice maintained much higher expression of *P22phox* and *Gp91phox* compared to that in young mice (increased by 63.45% and 112.27%, $P = 0.029$ and $P = 0.007$, respectively). In contrast, LF-treated mice exhibited a notable decrease in *P22phox* and *Gp91phox* expression (decreased by 31.19% and 33.56%, $P = 0.041$ and $P = 0.048$, respectively). These observations showed enhanced NADPH oxidase expression in the hippocampus of aged mice, and indicated the

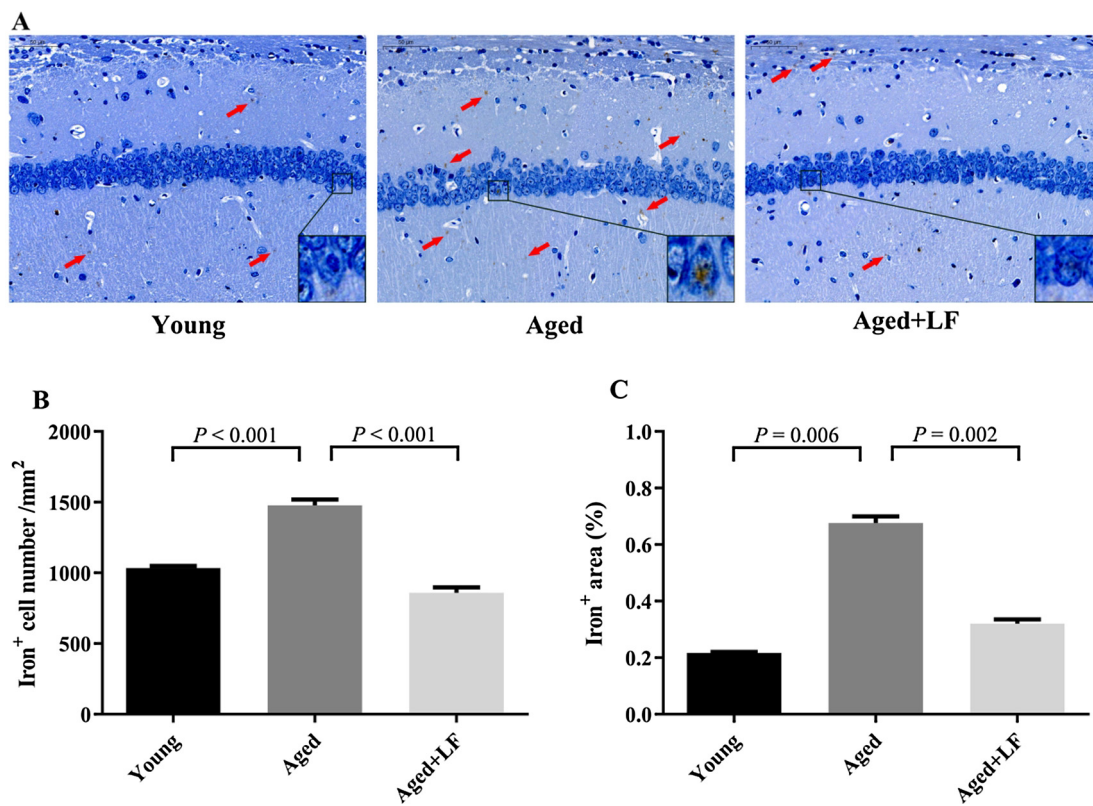


Fig. 3. Lactoferrin reduces iron deposits in the brain of aged mice. (A) Perl's staining showing iron deposition in the brain. The red arrowheads indicate iron deposits. Scale bar = 50 μm . (B) The numbers of iron-positive cells in the hippocampal CA1 subregion were counted (cells per mm^2) in three different fields (0.029 mm^2) of hippocampus sections. (C) Areas positive for iron staining were quantified and are shown as a percentage of the total surface area of the field. $n = 3$ mice per group.

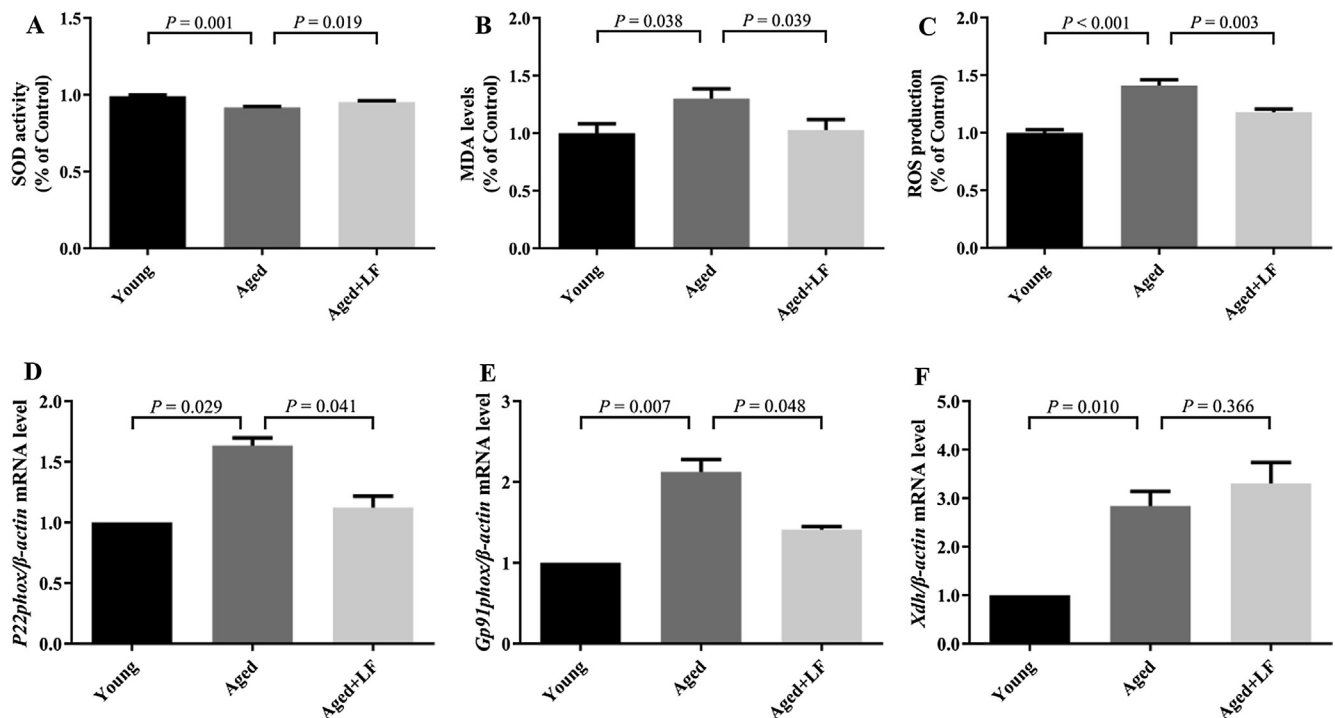


Fig. 4. Lactoferrin reduces oxidative stress in the hippocampus of aged mice. (A) SOD activity; (B) MDA levels; and (C) ROS production determined by ELISA. (D) *P22phox*, (E) *Gp91phox* and (F) *Xdh* gene expression levels determined by RT-qPCR. $n = 5$ mice per group.

ability of LF to partly reverse this situation.

Xanthine dehydrogenase (XDH) generates ROS as byproducts of purine metabolism; therefore, we also compared *Xdh* expression levels among the three groups. Compared with young mice, significantly higher levels of *Xdh* expressions were detected in the aged group (increased by 183.75%, $P = 0.01$; Fig. 4F), with no significant difference between the levels in the aged and aged + LF groups.

3.5. Local and universal inflammatory responses in aged mice were alleviated by LF administration

Inflammation has an adverse impact on cognition, and IL-1 β , IL-6 and TNF- α are closely associated with long-term potentiation (LTP) and synaptic plasticity (Özkorumak et al., 2019; Trapero & Cauli, 2014). To assess the inflammatory levels, we tested the hippocampal levels of proinflammatory cytokines of the three groups (Fig. 5). Aged mice had higher hippocampal levels of IL-1 β , IL-6 and TNF- α (increased by 167.42%, 73.00% and 84.39%, $P = 0.018$, $P = 0.008$ and $P = 0.026$ respectively), whereas LF administration partly reversed such trends (decreased by 76.39%, 58.52% and 50.67%, $P = 0.007$, $P = 0.003$ and $P = 0.019$, respectively). Furthermore, serum levels of these cytokines showed similar trends among the three groups, in which the aged group showed the highest levels of IL-1 β , IL-6 and TNF- α (increased by 32.49%, 65.10% and 40.96%, $P < 0.001$ for all three cytokines), whereas in mice treated with LF, we observed a decline in the levels of these cytokines (decreased by 11.92%, 17.03% and 14.01%, $P = 0.008$, $P = 0.016$ and $P = 0.012$, respectively). These findings indicate the ability of LF to reduce inflammatory responses in aged mice.

3.6. Metabolite changes in aged mice were partly reversed by LF administration

Next, we analyzed the differences in the metabolomic profiles of the hippocampus between the three groups. A total of 6634 metabolite features were detected in the positive mode and 5423 in the negative mode. Total ion chromatograms of hippocampus samples obtained from

the young, aged and aged + LF group are shown in [Supplementary materials 2 Fig. S1](#). PLS-DA models and heatmaps were used revealed pronounced differences in the metabolomic profiles among three groups (Fig. 6C and D). The PLS-DA model was validated by random permutation tests ([Supplementary materials 2 Fig. S2](#)). The statistically significant discriminant metabolites were chosen based on the remarkable differences in abundance (VIP > 1.0 and $P < 0.05$) identified in the young/aged and aged/aged + LF comparisons, and pairwise comparisons of the individual metabolites are shown in Fig. 7. Changes were found in some classes of lipids, such as lysophosphatidylglycerols (LysoPG 20:4, LysoPG 22:6), and lysophosphatidylserines (LysoPS 18:1), glycerol 1-hexadecanoate, docosapentaenoic acid, palmitelaidic acid, and tetracosapentaenoic acid (24:5n-3), which were increased in the aged group (increased by 79.43%, 117.49% and 84.09%, $P < 0.001$ for all three metabolites) and decreased (by 48.76%, 54.16% and 45.71%, $P < 0.001$ for all three metabolites) after LF intervention. Furthermore, xanthine and oxypurinol levels were increased in the brains of aged mice (by 32.19% and 55.55%, $P < 0.001$ for both two metabolites), whereas the adenosine level was lower in aged group (decreased by 38.08%, $P < 0.001$). These differences were partly reversed by LF administration: the levels of xanthine and oxypurinol were decreased by 25.04% and 27.95% ($P < 0.001$ and $P = 0.001$, respectively), and the level of adenosine was increased by 32.26% ($P = 0.045$), compared to the aged group, implying the ability of LF to reverse metabolic changes in the aged brain.

4. Discussion

In this study, we revealed the ability of LF to rescue aging-related cognitive deficits. Further investigations showed that LF treatment resulted in partial reversal of the age-related histological changes and less iron deposition in the hippocampus, with a concomitant reduction in ROS levels and universal inflammatory responses. Using LC-MS, we clarified the metabolomic alterations in aged brains, including increased levels of lysoPG, lysoPS, xanthine, adenosine and oxypurinol,

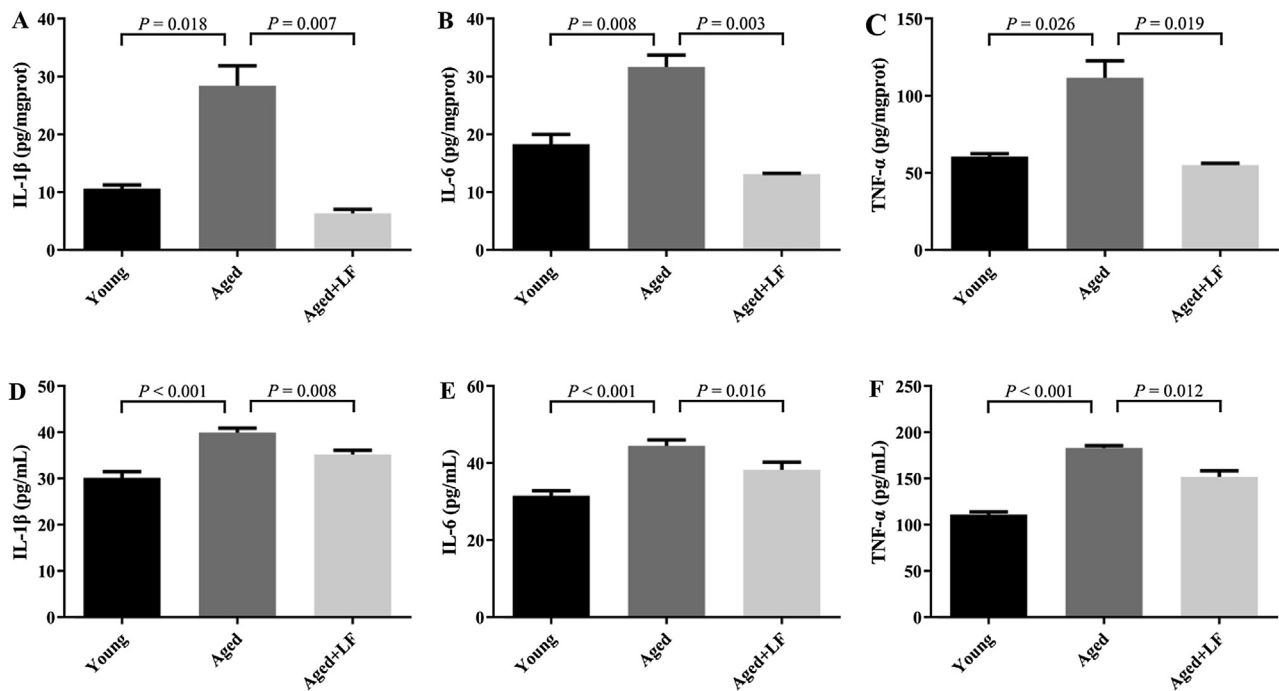


Fig. 5. Lactoferrin alleviates inflammatory responses in aged mice. (A) IL-1 β , (B) IL-6 and (C) TNF- α in hippocampus determined by ELISA (n = 5 mice per group). (D) IL-1 β , (E) IL-6 and (F) TNF- α in serum determined by ELISA (n = 10 mice per group).

which were partly reversed by LF administration.

Under normal physiological conditions, ROS exists in low concentrations and serve as important signaling messengers. However, ROS accumulation increases with ages (Davalli, Mitic, Caporali, Lauriola, & D'Arca, 2016). High concentrations of ROS are highly toxic to cells and contribute to the process of aging and age-related neurodegenerative diseases, such as Alzheimer's disease by inducing mitochondrial malfunction, impaired synaptic activity and neurotransmission, which eventually leading to cognitive deficits (Liochev, 2013; Tönnies & Trushina, 2017). Furthermore, as ROS mediates cellular damage, iron and ROS are perceived as "partners in crime" (Liochev & Fridovich, 1999). At high levels, iron is inherently toxic to neuronal cells, and generates ROS directly or through iron-chelated enzymes (Muñoz et al., 2016). In accordance with this, we showed increased iron deposition and upregulated expression of the ROS-generating enzymes, *P22phox*, *Gp91phox* and *Xdh* (increased by 63.45%, 112.27% and 183.75%, respectively), in the brains of aged mice. Furthermore, we found that excessive iron was not only deposited inside the neuronal cells, but also existed diffusely in the extracellular space, which indicated that iron exerts its adverse effects via multiple routes. This postulation is supported by the studies of Reinert and colleagues, in which more intense iron deposition was detected in glial cells than in neurons (Anja, Markus, Johannes, Thomas, & Tilo, 2019), leading to microglial hyperactivation and excessive ROS production in the CNS (Loane & Kumar, 2016; Yauger et al., 2019). By regulating iron homeostasis, LF is capable of decreasing ROS production (Kruzel, Zimecki, & Actor, 2017; Legrand, 2012; Moreno-Expósito et al., 2018). In its iron-free holoform, LF limits iron deposition in the brain by chelating ferric iron (Xu et al., 2019), and also inhibits ROS-generating enzymes (Mayeur, Spahis, Pouliot, & Levy, 2016; Part et al., 2015). As shown in the present study, the decrease in ROS levels in aged mice treated with LF was accompanied by a reduction in Fe³⁺ deposition, and concomitantly reduced expression of *P22phox* and *Gp91phox*.

Another phenomenon associated with ROS accumulation in aging is chronic low-grade inflammation (Fougère, Boulanger, Nourhashemi, Guyonnet, & Cesari, 2016), which also contributes to malfunctions of the brain and impaired cognition (Michaud et al., 2013). In our study,

LF administration in aged mice not only decreased iron deposition in the brain, but also reduced local IL-1 β , IL-6 and TNF- α levels, and decreased the universal levels of these three cytokines. Thus, it can be speculated that this immunoregulatory function is involved in the mechanism by which LF improves cognition in aged mice (Gonzalez-Chavez et al., 2009; Legrand, 2012; Mayeur et al., 2016). This hypothesis was further validated by our metabolomic analysis, in which aged mice exhibited increased concentrations LysoPG and LysoPS, whereas aged mice treated with LF exhibited a contrasting trend. Besides being components of cell membrane structure, LysoPS and LysoPG also facilitate the recruitment of inflammatory cells and its elevation is linked to intensified inflammation (Blankman, Long, Trauger, Siuzdak, & Cravatt, 2013; Frasch & Bratton, 2012). The relationships among LysoPS, LysoPG, inflammation, iron and ROS are reciprocal. The generation of LysoPS requires the function of NADPH oxidase and the presence of ROS (Frasch & Bratton, 2012), whereas prolonged exposure to inflammatory agents or iron elevates NADPH oxidase activity, which further exacerbates inflammation (Li & Frei, 2009). LF is known to suppress proinflammatory cytokine production by interacting with receptors on the membrane surface or targeting gene expression (Drago-Serrano et al., 2017), while boosting the release of anti-inflammatory cytokines, such as IL-10, IL-11, and IL-4 (Legrand, 2012).

In our metabolomic analysis, we found alterations in xanthine, oxypurinol and adenosine levels in aged brains compared with those detected in the young controls. We further analyzed the expression of *Xdh*, which is both a key enzyme in xanthine metabolism, and a contributor to ROS production (Berry & Hare, 2004). *Xdh* expression tends to increase with age (Vida et al., 2011), and this phenomenon was confirmed in the present study, although the LF treatment did not alter this trend. In addition, oxypurinol levels were increased in aged mice, which were reduced after LF intervention. Oxypurinol is an innate inhibitor of XDH, and acts to alleviate oxidative stress (Okafor, Farrington, & Gorog, 2017). Therefore, it seems somehow paradoxical that aged mice exhibited the highest levels of oxypurinol. This paradox might be explained by the ability of organisms to maintain redox homeostasis, which is an important mechanism of protection against physiological shifts in the level of oxidative stress (Rizvi, Kumar,

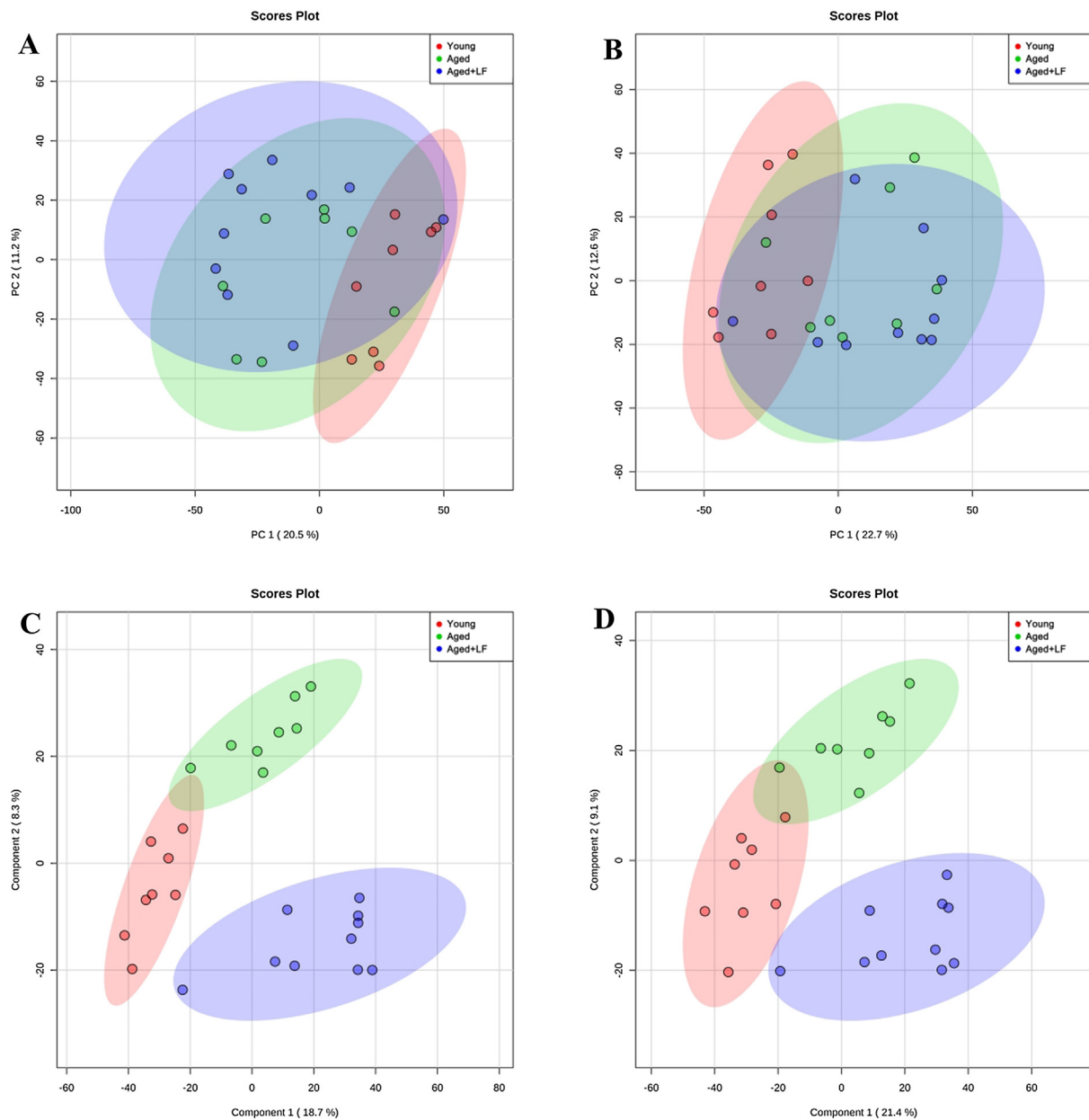


Fig. 6. Multivariate statistical analysis of metabolomic profiles of the hippocampus in the young, aged and aged + LF groups. PCA scores of groups in the (A) positive and (B) negative ion modes. PLS-DA scores of groups in the (C) positive and (D) negative ion modes.

Chakravarti, & Singh, 2011; Vida et al., 2011). Upregulation of these oxidative adaptation systems provides protection against acute insults, although repeated and chronic oxidative stress are eventually lethal (Pickering, Vojtovich, Tower, & Davies, 2013).

This study highlights several advantages of LF as a potential therapy for age-related cognitive impairment. First, as a natural protein derived from milk, LF is easily accessible and has few side-effects (Mayeur et al., 2016), a property confirmed in our previous study in which LF exhibited a wide spectrum of safe dose (Supplementary materials 1). Second, LF was shown to be effective in alleviating age-related cognitive decline via more than one mechanism as a result of its pleiotropic properties. Thus, the findings of this highlight potential new applications of LF both as a food supplement and a therapy for age-related cognitive decline.

5. Conclusion

Lactoferrin has been proved to be vital in early neurodevelopment and cognition (Chen et al., 2015; Wang, 2016), although the research on its potential in the aged brain is sparse. In this study, we showed that LF improves the cognitive ability of naturally aging C57/BL6J mice. Furthermore, LF reduces ROS production in the hippocampi of aged mice, which is associated with its effects on iron chelation and inflammatory regulation. We also provide some insights into the metabolomic changes induced in the brain by aging and LF intervention. This information will be important in designing therapeutic interventions aimed at alleviating age-related cognitive decline.

Ethics statement

All animal experiments in this research were in compliance with the ARRIVE guidelines and were carried out in accordance with the

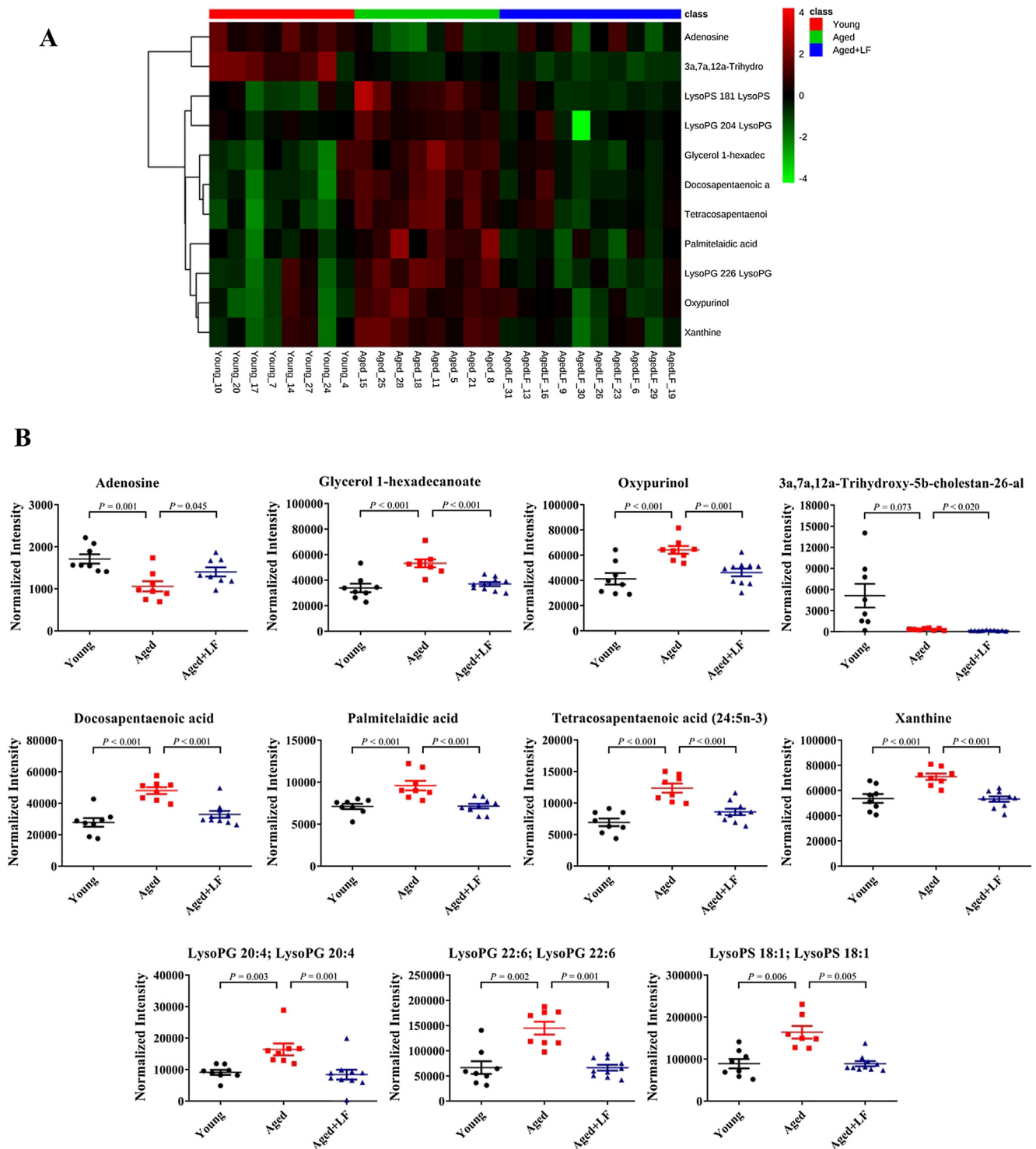


Fig. 7. Lactoferrin partly reverses metabolomic changes in aged mice. (A) Hierarchical clustering heatmap of the differential metabolites among the three groups. The color of each section is proportional to the significance of the changes in metabolites; red indicates upregulation and green indicates downregulation. (B) Changes in metabolite levels of hippocampus among three groups. The levels of metabolites were quantified and analyzed by one-way ANOVA. n = 8 mice per group.

National Institutes of Health Guide for the Care and Use of Laboratory Animals (NIH eighth edition, revised 2011) and Institutional Animal Care and Use Committee of Fujian Medical University (No. FJMU IACUC 2018-034).

Yunzhen Xie: Writing - Review & Editing. Fei Li: Data Curation. Yu Zhou: Resources. Liqin Qi: Resources. Libin Liu: Project Administration. Zhou Chen: Supervision.

CRedit authorship contribution statement

Declaration of Completing Interest

Jiaping Zheng: Conceptualization, Writing - Original Draft.

The authors declare that they have no known competing financial interests or personal relationships that could have appeared to

influence the work reported in this paper.

Acknowledgments

This work was supported by the National Natural Science Foundation of China (Grant No. 81800712), the Natural Science Foundation of Fujian Province, China (Grant No. 2018J01841) and the Research Fund of Fujian Provincial Key Laboratory of Natural Medicine Pharmacology (Grant No. FJNMP-201901).

The authors would like to thank Shuping Zheng and Junjin Lin from the Public Technology Service Center (Fujian Medical University, Fuzhou, China) for their technical assistance.

Appendix A. Supplementary material

Supplementary data to this article can be found online at <https://doi.org/10.1016/j.jff.2019.103736>.

References

- Anja, R., Markus, M., Johannes, S., Thomas, A., & Tilo, R. (2019). Iron concentrations in neurons and glial cells with estimates on ferritin concentrations. *BMC Neuroscience*, 20, 25.
- Au, A., Feher, A., McPhee, L., Jessa, A., Oh, S., & Einstein, G. (2016). Estrogens, inflammation and cognition. *Frontiers in Neuroendocrinology*, 40, 87–100.
- Bedard, K., & Krause, K. H. (2007). The NOX family of ROS-generating NADPH oxidases: Physiology and pathophysiology. *Physiological Reviews*, 87, 245–313.
- Berry, C. E., & Hare, J. M. (2004). Xanthine oxidoreductase and cardiovascular disease: Molecular mechanisms and pathophysiological implications. *Journal of Physiology (London, United Kingdom)*, 555, 589–606.
- Blankman, J. L., Long, J. Z., Trauger, S. A., Siuzdak, G., & Cravatt, B. F. (2013). ABHD12 controls brain lysophosphatidylserine pathways that are deregulated in a murine model of the neurodegenerative disease PHARC. *Proceedings of the National Academy of Sciences of the United States of America*, 110, 1500–1505.
- Chen, Y., Zheng, Z., Zhu, X., Shi, Y., Tian, D., Zhao, F., ... Wang, B. (2015). Lactoferrin promotes early neurodevelopment and cognition in postnatal piglets by upregulating the BDNF signaling pathway and polysialylation. *Molecular Neurobiology*, 52, 256–269.
- Daugherty, A. M., & Raz, N. (2015). Appraising the role of iron in brain aging and cognition: promises and limitations of MRI methods. *Neuropsychology Review*, 25, 272–287.
- Davalli, P., Mitic, T., Caporali, A., Lauriola, A., & D'Arca, D. (2016). ROS, cell senescence, and novel molecular mechanisms in aging and age-related diseases. *Oxidative Medicine and Cellular Longevity*, 2016, 3565127.
- Di Benedetto, S., Muller, L., Wenger, E., Duzel, S., & Pawelec, G. (2017). Contribution of neuroinflammation and immunity to brain aging and the mitigating effects of physical and cognitive interventions. *Neuroscience & Biobehavioral Reviews*, 75, 114–128.
- Dixon, S. J., & Stockwell, B. R. (2014). The role of iron and reactive oxygen species in cell death. *Nature Chemical Biology*, 10, 9.
- Dominique, L., Elizabeth, E., Mathireu, C., & Joel, M. (2006). Interactions of lactoferrin with cells involved in immune function. *Biochemistry and Cell Biology*, 84, 282–290.
- Drago-Serrano, M. E., Campos-Rodríguez, R., Carrero, J. C., & De, I. G. M. (2017). Lactoferrin: Balancing Ups and Downs of Inflammation Due to Microbial Infections. *International Journal of Molecular Sciences* 18, 501.
- Erika B. W., & Steven S. S. (2013). Ageing alters perivascular nerve function of mouse mesenteric arteries in vivo. *The Journal of Physiology*, 591, 1251–1263.
- Fougère, B., Boulanger, E., Nourhashemi, F., Guyonnet, S., & Cesari, M. (2016). Chronic inflammation: Accelerator of biological aging. *Journals of Gerontology*, 72, 1218–1225.
- Frasch, S. C., & Bratton, D. L. (2012). Emerging roles for lysophosphatidylserine in resolution of inflammation. *Progress in Lipid Research*, 51, 199–207.
- Gonzalez-Chavez, S. A., Arevalo-Gallegos, S., & Rascon-Cruz, Q. (2009). Lactoferrin: Structure, function and applications. *International Journal of Antimicrobial Agents*, 33(301), e301–308.
- Guo, C., Yang, Z. H., Zhang, S., Chai, R., Xue, H., Zhang, Y. H., ... Wang, Z. Y. (2017). Intranasal lactoferrin enhances alpha-secretase-dependent amyloid precursor protein processing via the ERK1/2-CREB and HIF-1alpha Pathways in an Alzheimer's disease mouse model. *Neuropsychopharmacology*, 42, 2504–2515.
- Guo, H. Y., Jiang, L., Ibrahim, S. A., Zhang, L., Zhang, H., Zhang, M., & Ren, F. Z. (2009). Orally administered lactoferrin preserves bone mass and microarchitecture in ovariectomized rats. *Journal of Nutrition*, 139, 958–964.
- Guzik, T. J., & Touyz, R. M. (2017). Oxidative stress, inflammation, and vascular aging in hypertension. *Hypertension*, 70, 660.
- Hou, J. M., Xue, Y., & Lin, Q. M. (2012). Bovine lactoferrin improves bone mass and microstructure in ovariectomized rats via OPG/RANKL/RANK pathway. *Acta Pharmaceutica Sinica*, 33, 1277–1284.
- Jasmine, C., Mai, Y., & Jianguo, X. (2019). MetaboAnalystR 2.0: From raw spectra to biological insights. *Metabolites*, 9, 57.
- Kell, D. B. (2009). Iron behaving badly: Inappropriate iron chelation as a major contributor to the aetiology of vascular and other progressive inflammatory and degenerative diseases. *BMC Medical Genomics*, 2, 2.
- Kruzal, M. L., Zimecki, M., & Actor, J. K. (2017). Lactoferrin in a context of inflammation-induced pathology. *Frontiers in Immunology*, 8, 1438.
- Legrand, D. (2012). Lactoferrin, a key molecule in immune and inflammatory processes. *Biochemistry and Cell Biology*, 90, 252–268.
- Li, L., & Frei, B. (2009). Prolonged exposure to LPS increases iron, heme, and p22phox levels and NADPH oxidase activity in human aortic endothelial cells: Inhibition by desferrioxamine. *Arteriosclerosis, Thrombosis, and Vascular Biology*, 29, 732–738.
- Liochev, S. I. (2013). Reactive oxygen species and the free radical theory of aging. *Free Radical Biology & Medicine*, 60, 1–4.
- Liochev, S. I., & Fridovich, I. (1999). Superoxide and iron: Partners in crime. *IUBMB Life*, 48, 157–161.
- Loane, D. J., & Kumar, A. (2016). Microglia in the TBI brain: The good, the bad, and the dysregulated. *Experimental Neurology*, 275, 316–327.
- Mattson, M. P., & Magnus, T. (2006). Ageing and neuronal vulnerability. *Nature Reviews Neuroscience*, 7, 278.
- Mayer, S., Spahis, S., Pouliot, Y., & Levy, E. (2016). Lactoferrin, a pleiotropic protein in health and disease. *Antioxidants & Redox Signaling*, 24, 813–836.
- Michaud, M., Balardy, L., Moulis, G., Gaudin, C., Peyrot, C., Vellas, B., ... Nourhashemi, F. (2013). Proinflammatory cytokines, aging, and age-related diseases. *Journal of the American Medical Directors Association*, 14, 877–882.
- Moldogazieva, N. T., Mokhosoev, I. M., Mel'nikova, T. I., Porozov, Y. B., & Terentiev, A. A. (2019). Oxidative stress and Advanced Lipoxidation and Glycation End Products (ALEs and AGEs) in aging and age-related diseases. *Oxidative Medicine and Cellular Longevity*, 2019, 3085756.
- Moreno-Expósito, L., Illescas-Montes, R., Melguizo-Rodríguez, L., Ruiz, C., Ramos-Torrecillas, J., & Luna-Bertos, E. D. (2018). Multifunctional capacity and therapeutic potential of lactoferrin. *Life Sciences*, 195, 61–64.
- Muñoz, Y., Carrasco, C. M., Campos, J. D., Aguirre, P., & Núñez, M. T. (2016). Parkinson's disease: The mitochondria-iron link. *Parkinson's Disease*, 2016, 1–21.
- Okafor, O. N., Farrington, K., & Gorog, D. A. (2017). Allopurinol as a therapeutic option in cardiovascular disease. *Pharmacology & Therapeutics*, 172, 139–150.
- Özkorumak, K. E., Civil, A. F., Korkmaz, U. E., Selim, D., Sağlam, A. D., Mustafa, T., & Süleyman, K. (2019). Blood levels of interleukin-1 beta, interleukin-6 and tumor necrosis factor-alpha and cognitive functions in patients with obsessive compulsive disorder. *Comprehensive Psychiatry*, 89, 61–66.
- Park, Y. G., Jeong, J. K., Lee, J. H., Lee, Y. J., Seol, J. W., Kim, S. J., ... Park, S. Y. (2013). Lactoferrin protects against prion protein-induced cell death in neuronal cells by preventing mitochondrial dysfunction. *International Journal of Molecular Medicine*, 31, 325–330.
- Part, K., Kunis-Beres, K., Poska, H., Land, T., Shimmo, R., & Zetterstrom Fernaeus, S. (2015). Amyloid beta25-35 induced ROS-burst through NADPH oxidase is sensitive to iron chelation in microglial Bv2 cells. *Brain Research*, 1629, 282–290.
- Pickering, A. M., Vojtovich, L., Tower, J., & Davies, K. J. A. (2013). Oxidative stress adaptation with acute, chronic, and repeated stress. *Free Radical Biology & Medicine*, 55, 109–118.
- Plain, K. M., Marsh, I. B., Waldron, A. M., Galea, F., Whittington, A. M., Saunders, V. F., ... Whittington, R. J. (2014). High-throughput direct fecal PCR assay for detection of *Mycobacterium avium* subsp. *paratuberculosis* in sheep and cattle. *Journal of Clinical Microbiology*, 52, 745–757.
- Rizvi, S. I., Kumar, D., Chakravarti, S., & Singh, P. (2011). Erythrocyte plasma membrane redox system may determine maximum life span. *Medical Hypotheses*, 76, 547–549.
- Sala-Llonch, R., Idland, A.-V., Borza, T., Watne, L. O., Wyller, T. B., Brækhus, A., ... Martin Fjell, A. (2017). Inflammation, amyloid, and atrophy in the aging brain: Relationships with longitudinal changes in cognition. *Journal of Alzheimer's Disease*, 58, 1–12.
- Saraswat, K., & Rizvi, S. I. (2017). Novel strategies for anti-aging drug discovery. *Expert Opinion on Drug Discovery*, 12, 955–966.
- Tönnies, E., & Trushina, E. (2017). Oxidative stress, synaptic dysfunction, and Alzheimer's disease. *Journal of Alzheimer's Disease*, 57, 1105–1121.
- Toshitaka, N., Isao, N., & Hidenori, I. (2019). Iron homeostasis and iron-regulated ROS in cell death, senescence and human diseases. *Biochimica et Biophysica Acta, General Subjects*, 1863, 1398–1409.
- Trapero, I., & Cauli, O. (2014). Interleukin 6 and cognitive dysfunction. *Metabolic Brain Disease*, 29, 593–608.
- van der Strate, B. W., Beljaars, L., Molema, G., Harmsen, M. C., & Meijer, D. K. (2001). Antiviral activities of lactoferrin. *Antiviral Research*, 52, 225–239.
- Vida, C., Rodriguez-Teres, S., Heras, V., Corpas, I., De la Fuente, M., & Gonzalez, E. (2011). The aged-related increase in xanthine oxidase expression and activity in several tissues from mice is not shown in long-lived animals. *Biogerontology*, 12, 551–564.
- Vorhees, C. V., & Williams, M. T. (2006). Morris water maze: Procedures for assessing spatial and related forms of learning and memory. *Nature Protocols*, 1, 848–858.
- Wang, B. (2016). Molecular determinants of milk lactoferrin as a bioactive compound in early neurodevelopment and cognition. *Journal of Pediatrics*, 173, S29–36.
- Wang, Y., & Hekimi, S. (2015). Mitochondrial dysfunction and longevity in animals: Untangling the knot. *Science*, 350, 1204–1207.
- Wyss-Coray, T. (2016). Ageing, neurodegeneration and brain rejuvenation. *Nature*, 539, 180–186.
- Xin-wei, C., Ye-hong, L., Meng-jun, Z., Zhou, C., Dian-shan, K., Ying, X., & Jian-ming, H. (2019). Lactoferrin ameliorates aging-suppressed osteogenesis via IGF1 signaling. *Journal of Molecular Endocrinology*, 63, 63–75.
- Xu, S.-F., Zhang, Y.-H., Wang, S., Pang, Z.-Q., Fan, Y.-G., Li, J.-Y., ... Guo, C. (2019). Lactoferrin ameliorates dopaminergic neurodegeneration and motor deficits in MPTP-treated mice. *Redox Biology*, 21, 101090.
- Yan, L., Michel, N., Anne, R., & Bernard, M. (2019). Metal ions in Alzheimer's disease: A key role or not? *Accounts of Chemical Research*, 52, 2026–2035.
- Yauger, Y. J., Bermudez, S., Moritz, K. E., Glaser, E., Stoica, B., & Byrnes, K. R. (2019). Iron accentuated reactive oxygen species release by NADPH oxidase in activated microglia contributes to oxidative stress in vitro. *Journal of Neuroinflammation*, 16, 41.
- Zucca, F. A., Segura-Aguilar, J., Ferrari, E., Muñoz, P., Paris, I., Sulzer, D., ... Zecca, L. (2017). Interactions of iron, dopamine and neuromelanin pathways in brain aging and Parkinson's disease. *Progress in Neurobiology*, 155, 96.